International Journal of Latest Research in Engineering and Technology (IJLRET)
ISSN: 2454-5031
www.ijlret.com || Volume 12 - Issue 06 || June 2026 || PP. 11-17

Scattering-induced enhancement of color uniformity in white LEDs using ZrC phosphor

Nguyen Thi Phuong Loan[1*]
[1]*Faculty of Fundamental 2, Posts and Telecommunications Institute of Technology, Ho Chi Minh City, Vietnam*
**Corresponding Author*

Abstract: Transition-metal carbide/nitride multilayer coatings have attracted significant interest due to their excellent combination of hardness, wear resistance, thermal stability, and chemical durability. In this study, multilayer coatings were synthesized using an energetic thin-film deposition technique and subsequently characterized to evaluate their structural, mechanical, and tribological properties. The multilayer architecture promoted the formation of dense nanocrystalline structures with strong interfacial bonding between adjacent layers. The coatings exhibited enhanced mechanical performance compared with conventional single-layer counterparts, owing to the combined effects of interface strengthening and grain refinement. Furthermore, the multilayer configuration contributed to improved wear resistance and reduced friction during sliding contact. The results demonstrate that carbide/nitride multilayers are promising candidates for advanced protective coating applications requiring high mechanical reliability and long-term durability.
Keywords: Angular color uniformity, Color quality scale, Correlated color temperature, Light scattering, White LEDs, ZrC phosphor.

I. Introduction

Transition-metal carbides and nitrides are widely recognized as important protective coating materials because of their exceptional hardness, excellent wear resistance, high melting temperatures, and outstanding chemical stability[1–3]. These properties have led to their extensive application in cutting tools, mechanical components, protective surfaces, and other engineering systems operating under demanding conditions.To further improve coating performance, various strategies have been explored, including alloying, multicomponent compounds, and multilayer architectures[4–6]. Among these approaches, multilayer coatings have received considerable attention because the introduction of multiple interfaces can effectively enhance mechanical strength while preserving the intrinsic properties of the constituent materials. Such structures are particularly attractive for applications that require both functional stability and superior mechanical durability.Energetic deposition techniques have proven effective for producing high-quality multilayer coatings. These methods facilitate the growth of dense films with strong adhesion and refined microstructures, even under relatively moderate processing conditions. Consequently, multilayer carbide/nitride systems continue to be investigated as promising materials for advanced surface engineering applications[7].

II. Experimental Details

Multilayer coatings consisting of alternating carbide and nitride layers were deposited onto silicon substrates using a thin-film deposition technique based on energetic plasma species. The deposition parameters were carefully controlled to ensure stable film growth and uniform layer formation throughout the multilayer structure.The structural characteristics of the deposited coatings were evaluated using complementary microstructural and compositional characterization techniques. Mechanical properties were investigated through nanoindentation measurements, while tribological behavior was assessed using wear and friction testing under controlled loading conditions. Additional analyses were performed to examine coating integrity and interfacial stability following mechanical loading[8–10].

III. Discussion

The deposited multilayer coatings exhibited dense microstructures and well-defined layer architectures. Interfacial regions between neighboring layers showed evidence of atomic-scale interactions, which contributed to strong bonding throughout the multilayer stack. Such interfacial characteristics are beneficial for improving the structural integrity of multilayer coatings. The refined microstructure of the coatings played an important role in enhancing mechanical performance. The combination of nanoscale grain structures and a high density of interfaces provided effective barriers to deformation mechanisms, resulting in improved hardness and mechanical stability. Compared with conventional monolithic coatings, multilayer structures generally offer superior resistance to plastic deformation due to interface-related strengthening effects. Tribological investigations demonstrated favorable wear behavior and relatively low friction characteristics. The multilayer architecture contributed to maintaining coating integrity during repeated contact and sliding conditions. The presence of multiple interfaces can suppress crack initiation and retard crack propagation, thereby improving resistance to wear-induced damage. The enhanced mechanical and tribological performance of the coatings can be attributed to the synergistic effects of microstructural refinement, interface strengthening, and strong adhesion between the coating and substrate. These factors collectively contribute to improved durability and reliability under mechanical loading[11–13].

The particle size distribution and scattering characteristics of the ZrC phosphor are illustrated in Figure 1. The particle diameter exhibits a nearly Gaussian distribution centered around 1 μm, indicating a relatively uniform particle morphology. As the ZrC concentration increases from 1 wt.% to 13 wt.%, the scattering coefficient increases significantly throughout the visible wavelength region. Moreover, a gradual increase in reduced scattering coefficient is also observed at all investigated wavelengths. The enhanced scattering behavior can be attributed to the higher density of scattering centers introduced by the additional ZrC particles. Consequently, light propagation inside the phosphor layer becomes more diffusive, promoting stronger optical mixing and improved angular color uniformity. To maintain the target correlated color temperature of 5000 K, the concentration of YAG^{3+} phosphor was gradually reduced with increasing ZrC concentration, as shown in Figure 2. The YAG^{3+} content decreases almost linearly from approximately 12.8 wt.% to about 7.2 wt.% when the ZrC concentration increases from 1 wt.% to 13 wt.%. This trend suggests that the optical contribution of ZrC partially compensates for the yellow emission generated by YAG^{3+}, allowing the phosphor composition to be adjusted while preserving the desired white-light characteristics[14–17].The angular CCT distributions presented in Figure 3 reveal a noticeable influence of ZrC concentration on color uniformity. At low phosphor concentrations, the CCT variation between the central and peripheral viewing angles is relatively large. However, as the ZrC content increases, the angular CCT curves become flatter, indicating a more homogeneous color distribution. The improved angular uniformity originates from enhanced scattering processes that facilitate more effective spectral mixing within the phosphor layer. This observation is further confirmed by the ΔCCT values shown in Figure 4. Although some fluctuations occur at intermediate concentrations, the overall tendency indicates that higher ZrC concentrations reduce color deviation. The lowest ΔCCT values are generally obtained at concentrations above 8 wt.%, demonstrating superior color homogeneity. The reduction in color deviation can be attributed to the stronger scattering effect, which minimizes spatial separation between different spectral components[18–21].

The luminous flux characteristics of the WLED package are presented in Figure 5. Unlike conventional phosphor additions that may increase optical extraction, the incorporation of ZrC leads to a gradual reduction in luminous flux. Specifically, the luminous output decreases from approximately 136 lm at 1 wt.% ZrC to around 113 lm at 13 wt.% ZrC. This reduction is primarily associated with increased optical scattering and absorption losses within the phosphor layer. At higher concentrations, photons experience longer propagation paths and a greater probability of reabsorption, resulting in lower light extraction efficiency[22–25].

The influence of ZrC concentration on color-rendering performance is shown in Figures 6 and 7. Figure 6 demonstrates that the CRI decreases slightly from approximately 70 to 69 as the ZrC concentration increases. Although the reduction is relatively small, it indicates a gradual imbalance in the spectral distribution caused by excessive scattering and modifications in phosphor composition. Nevertheless, the CRI remains relatively stable throughout the investigated concentration range. A similar trend can be observed for the color quality scale (CQS) in Figure 7. The CQS initially increases and reaches its maximum value of approximately 66 at around 9 wt.% ZrC, indicating improved overall color quality. Beyond this concentration, the CQS gradually decreases and stabilizes near 64–65. This behavior suggests that moderate ZrC loading improves color quality through enhanced spectral mixing, whereas excessive concentrations may introduce optical losses and spectral imbalance.

The emission spectra of the ZrC-based WLED package are shown in Figure 8. Two dominant spectral regions can be identified, consisting of the blue emission from the LED chip and the broad phosphor-converted emission centered in the visible region. As the ZrC concentration increases, the intensity of the converted emission band gradually rises, while the blue component remains sufficiently strong to maintain white-light generation. The enhanced visible emission indicates improved photon conversion and redistribution within the phosphor layer. Combined with the increased scattering capability of ZrC particles, these spectral modifications contribute significantly to the observed improvements in color uniformity and color quality[26-31].

Overall, the incorporation of ZrC phosphor enhances optical scattering and angular color uniformity while maintaining acceptable color-rendering performance. Although excessive ZrC concentrations may reduce luminous flux, an intermediate concentration range of approximately 8–10 wt.% appears to provide the best compromise between color uniformity, color quality, and optical efficiency.

International Journal of Latest Research in Engineering and Technology (IJLRET)
ISSN: 2454-5031
www.ijlret.com || Volume 12 - Issue 06 || June 2026 || PP. 11-17

IV. Figures and Tables

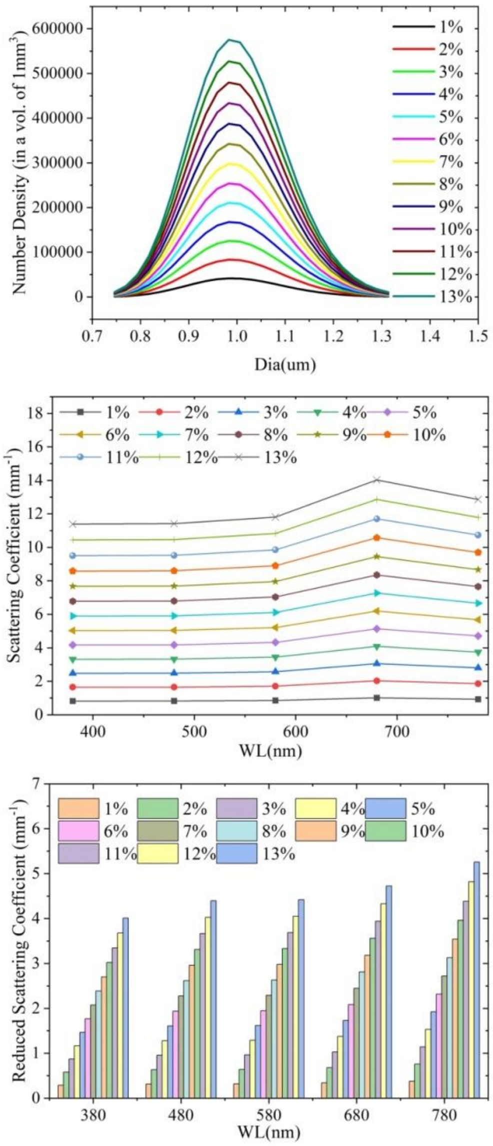

Fig. 1: Particle size distribution and scattering coefficient of ZrC phosphor particles at different concentrations in the phosphor layer.

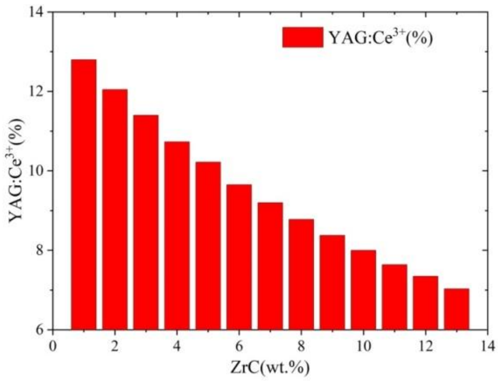

Fig. 2: Variation of YAG:Ce^{3+} phosphor concentration as a function of ZrC phosphor content for maintaining a correlated color temperature of 5000 K.

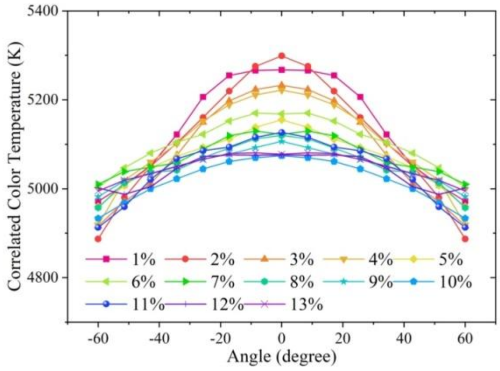

Fig. 3: Angular correlated color temperature (CCT) distribution of the ZrC-based WLED at different phosphor concentrations.

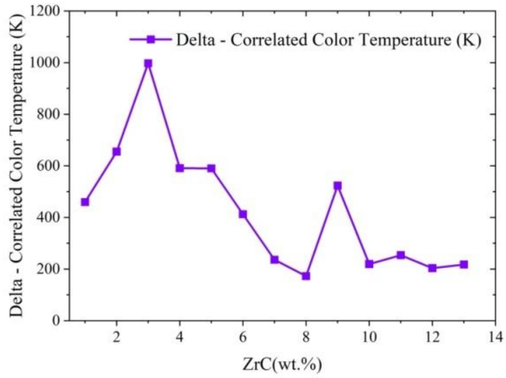

Fig. 4: Color deviation (ΔCCT) of the ZrC-based WLED as a function of ZrC phosphor concentration.

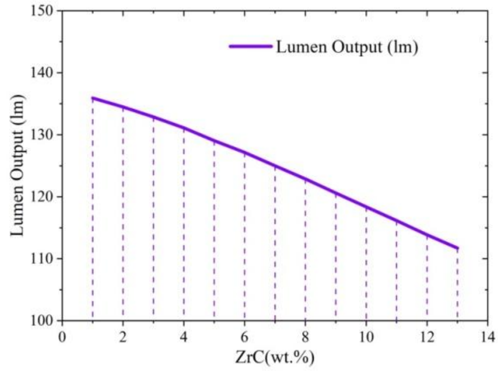

Fig. 5: Luminous flux of the ZrC-based WLED versus ZrC phosphor concentration.

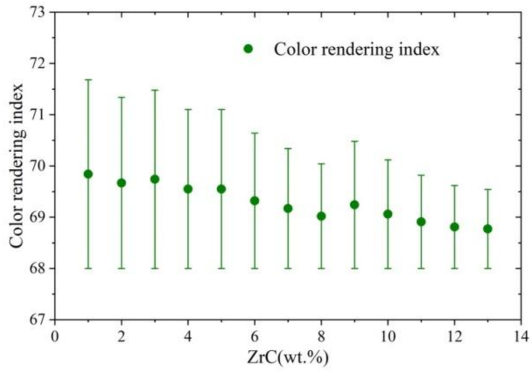

Fig. 6: Variation of color rendering index (CRI) with ZrC phosphor concentration.

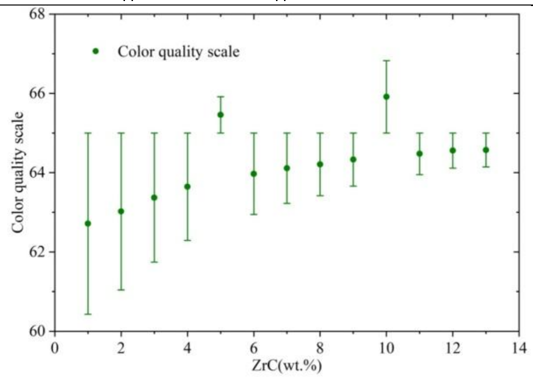

Fig. 7: Variation of color quality scale (CQS) with ZrC phosphor concentration.

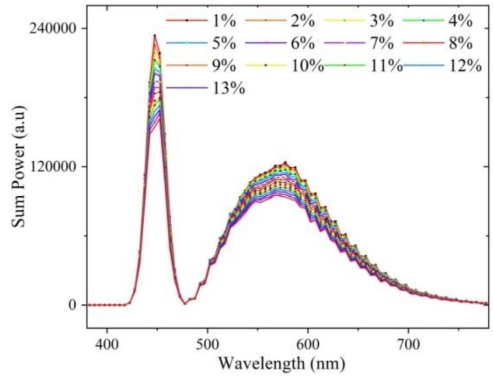

Fig. 8: Emission spectra of the ZrC-based WLED package under different ZrC phosphor concentrations.

V. Conclusion

Multilayer carbide/nitride coatings exhibited excellent potential as protective surface materials due to their favorable combination of hardness, wear resistance, and structural stability. The multilayer architecture promoted strong interfacial bonding and refined microstructures, both of which contributed significantly to the observed mechanical performance. The incorporation of multiple interfaces provided effective strengthening mechanisms and enhanced resistance to tribological damage. Furthermore, the dense nature of the deposited coatings contributed to improved durability and coating integrity during mechanical loading. These findings highlight the advantages of multilayer carbide/nitride systems for advanced engineering applications requiring reliable long-term surface protection.

VI. Acknowledgements

The authors wish to express their gratitude to the Posts and Telecommunications Institute of Technology, Vietnam, for financial support for this research.

References

[1] Anh, N.D.Q.; Loan, N.T.P.; Van De, P.; Lee, H. (2025). Potassium Bromide scattering simulation for improving phosphor-converting white LED performance. Optoelectronics and Advanced Materials – Rapid Communications, 19(7–8), 378–383.

[2] Francis, K.J.; Boink, Y.E.; Dantuma, M.; Singh, M.K.A.; Manohar, S.; Steenbergen, W. (2020). Tomographic imaging with an ultrasound and LED-based photoacoustic system. Biomedical Optics Express, 11(4), 2152–2165.

[3] Lin, S.-H. et al. (2021). Enhanced external quantum efficiencies of AlGaN-based deep-UV LEDs using reflective passivation layer. Optics Express, 29(23), 37835–37844.

[4] Loan, N.T.P.; Anh, N.D.Q.; Man, P.T.M.; Lee, H.-Y. (2025). Assessing Thermic Degradation for Yttrium–Aluminum Precursive Agents Applied to YAG Phosphor Samples. Science and Technology Indonesia, 10(4), 1209–1214.

[5] Li, J. et al. (2021). On-chip integration of III-nitride flip-chip light-emitting diodes with photodetectors. Journal of Lightwave Technology, 39(8), 2603–2608.

[6] Tsai, C.-M.; Chang, C.-S.; Xu, Z.; Huang, W.-P.; Lai, W.-C.; Bow, J.-S. (2019). Efficiency enhancement of III-nitride light-emitting diodes with strain-compensated thin-barrier InGaN/AlN/GaN multiple quantum wells. OSA Continuum, 2(4), 1207–1214.

[7] Chlipala, M. et al. (2020). Nitride light-emitting diodes for cryogenic temperatures. Optics Express, 28(20), 30299–30308.

[8] Loan, N.T.P.; Man, P.T.M.; Le, P.X. (2026). Non-Proximity as Well as Immediate Tracking for Phosphor Heat Within Phosphor-Transmuted WLED Apparatuses. Indonesian Journal of Material Research, 4(2).

[9] Tian, K. et al. (2019). On the polarization self-screening effect in multiple quantum wells for nitride-based near ultraviolet light-emitting diodes. Chinese Optics Letters, 17(12), 122301.

[10] Hassan, A.; Khan, S.; Rasul, K.; Hussain, A. (2020). Lensless on-chip LED array microscope using amplitude and phase masks. Journal of the Optical Society of America B, 37(12), 3652–3659.

[11] Gao, X. et al. (2021). Circularly polarized light emission from a GaN micro-LED integrated with functional metasurfaces for 3D display. Optics Letters, 46(11), 2666–2669.

[12] Zhang, S. et al. (2020). Efficient emission of InGaN-based light-emitting diodes: toward orange and red. Photonics Research, 8(11), 1671–1675.

[13] Zhang, T.; Zhang, X.; Ding, B.; Shen, J.; Hu, Y.; Gu, H. (2020). Homo-epitaxial secondary growth of ZnO nanowire arrays for a UV-free warm white light-emitting diode application. Applied Optics, 59(8), 2498–2504.

[14] Goo, H.; Mo, S.; Park, H.J.; Lee, M.Y.; Ahn, J.-C. (2021). Treatment with LEDs at a wavelength of 642 nm enhances skin tumor proliferation in a mouse model. Biomedical Optics Express, 12(9), 5583–5596.

[15] Treviño, M.V.; Gutiérrez, J.G.; Lelis, J.M.R.; Apreza, E.L. (2020). Optimizing an LED array for an infrared illumination source using the near field for venous pattern detection. Applied Optics, 59(9), 2858–2865.

[16] Su, V.-C.; Gao, C.-C. (2020). Remote GaN metalens applied to white light-emitting diodes. Optics Express, 28(26), 38883–38891.

[17] Griffiths, A.D. et al. (2019). Multispectral time-of-flight imaging using light-emitting diodes. Optics Express, 27(24), 35485–35498.

[18] Xu, Z.-H.; Chen, W.; Penuelas, J.; Padgett, M.; Sun, M.-J. (2018). 1000 fps computational ghost imaging using LED-based structured illumination. Optics Express, 26(3), 2427–2434.

[19] Hedili, M.K.; Soner, B.; Ulusoy, E.; Urey, H. (2019). Light-efficient augmented reality display with steerable eyebox. Optics Express, 27(9), 12572–12581.

[20] Anas, E.M.A.; Zhang, H.K.; Kang, J.; Boctor, E. (2018). Enabling fast and high quality LED photoacoustic imaging: a recurrent neural networks based approach. Biomedical Optics Express, 9(8), 3852–3866.

[21] Khan, M.A.; Takeda, R.; Yamada, Y.; Maeda, N.; Jo, M.; Hirayama, H. (2020). Beyond 53% internal quantum efficiency in a AlGaN quantum well at 326 nm UVA emission and single-peak operation of UVA LED. Optics Letters, 45(2), 495–498.

[22] Gu, H.; Chen, M.; Wang, Q.; Tan, Q. (2018). Design of two-dimensional diffractive optical elements for beam shaping of multicolor light-emitting diodes. Applied Optics, 57(10), 2653–2658.

[23] Hsiang, E.-L.; Yang, Q.; He, Z.; Zou, J.; Wu, S.-T. (2020). Halo effect in high-dynamic-range mini-LED backlit LCDs. Optics Express, 28(24), 36822–36837.

[24] Chen, D. et al. (2021). Improved electro-optical and photoelectric performance of GaN-based micro-LEDs with an atomic layer deposited AlN passivation layer. Optics Express, 29(22), 36559–36566.

[25] Wang, W.; Zhu, P. (2018). Red photoluminescent Eu^{3+}-doped Y_2O_3 nanospheres for LED-phosphor applications: synthesis and characterization. Optics Express, 26(26), 34820–34829.

[26] Chung, K.; Sui, J.; Sarwar, T.; Ku, P.-C. (2019). Feasibility study of nanopillar LED array for color-tunable lighting and beyond. Optics Express, 27(26), 38229–38235.

[27] Anh, N.D.Q.; Ho, S.D.; Man, P.T.M.; Duy, T.K.; Loan, N.T.P. (2025). Obtaining higher LED's lighting chromaticity and luminosity with SiO_2 particles at different diameters. Journal of Advanced Engineering and Computation, 9(1), 21–28.

[28] Anh, N.D.Q.; Lee, H.Y. (2024). Titanium dioxide in vanadate red phosphor compound for conventional white light emitting diodes. Optoelectronics and Advanced Materials – Rapid Communications, 18, 480–484.

[29] Cong, P.H.; Anh, N.D.Q. (2025). Augmenting Chroma Performance for WLED Employing $Sr_8ZnSc(PO_4)_7:Eu^{2+}@SiO_2$ as a Scattering-Enhancing Substance. Science and Technology Indonesia, 10(2), 467–472.

[30] Loan, N.T.P.; Lee, H.-Y.; Man, P.T.M. (2026). Structural and Optical Properties of Co-Doped ZnO Nanoparticles Synthesized by the Sol-Gel Method. Indonesian Journal of Material Research, 4(3).

[31] Loan, N.T.P.; Le, P.X.; Man, P.T.M. (2026). Photoluminescence Broadening Induced by Internal Electric Field Variations in Polar InGaN/GaN Quantum Wells. Indonesian Journal of Material Research, 4(3).